Structural Monitoring and Maintenance, *Vol. 11, No. 4 (2024) 277-296*
https://doi.org/10.12989/smm.2024.11.4.277

Investigating measures to improve seismic performance of stone arch bridges using larger filling stones

Aiko Furukawa* and Yusuke Higashi

Department of Urban Management, Graduate School of Engineering, Kyoto University, Kyotodaigaku-katsura, Nishikyo-ku, Kyoto-shi, Kyoto 615-8540, Japan

(*Received August 8, 2024, Revised October 17, 2024, Accepted November 3, 2024*)

Abstract. Stone arch bridges in Japan consist of ring stones, wall stones, and filling material. Some stone arch bridges have a filling material of small size, while others have a filling material of large size. During past earthquakes, the filling material collapsed and made the wall stones to collapse together, therefore, the stability of the filling material itself seems to have an important influence on the seismic performance of stone arch bridges. However, few studies have investigated the filling material. This study focused on the effect of the filling material size on the seismic performance of stone arch bridges. The seismic behavior of stone arch bridges with large or small crushed stones as the filling material was compared through shaking table tests and numerical simulation using the refined distinct element method. The shaking table test revealed that the natural frequencies and resonance curves of stone arch bridges with large and small crushed stones are similar. However, the seismic performance was different depending on the size of crushed stone. The stone arch bridge with larger crushed stones withstood the earthquake shaking for longer time. The post-collapse appearance of the test specimen revealed that large crushed stones were more stable than small crushed stones, because large crushed stones stabilized with a steeper slope angle. The numerical simulation revealed a trend similar to that in the shaking table test. The results revealed that replacing the filling material with larger stones is expected to improve seismic performance in the maintenance of stone arch bridges.

Keywords: DEM; filling material size; seismic performance; shaking table test; stone arch bridge

1. Introduction

Construction techniques for stone arch bridges were introduced to Japan from overseas approximately 400 years ago, and stone arch bridges have since been widely built across Japan, particularly in the Kyushu region (Nigeme and Yoshihara 2001). Currently, approximately 3000 stone arch bridges support human activity. While serving as essential components of social infrastructure, many stone arch bridges are designated as cultural heritage, owing to their historical value and the aesthetic beauty of their arch shapes. However, these stone arch bridges have experienced damage during past earthquakes, particularly during the 2016 Kumamoto earthquake.

Owing to the historical and cultural significance of stone arch bridges, post-earthquake restoration is required, and stone arch bridges must often be restored to their original state to

*Corresponding author, Associate Professor, E-mail: furukawa.aiko.3w@kyoto-u.ac.jp

http://www.techno-press.org/?journal=smm&subpage=7 ISSN: 2288-6605 (Print), 2288-6613 (Online)

preserve cultural heritage. Effective rehabilitation and restoration methods are needed to improve seismic performance without reducing cultural value. However, the identification of effective methods remains challenging.

The major components of stone arch bridges in Japan are ring stones, wall stones, and filling materials. During the 2016 Kumamoto earthquake, there was little damage to the ring stones, and most damage was caused by the collapse of wall stones (Japan Society of Civil Engineers, 2017). At the Futamata-Fukura Bridge, the filling material and wall stones collapsed together, and it appeared that the collapse of filling material caused the collapse of the wall stones.

Filling material varies among different bridges. In many cases, filling material is a mixture of gravel and soil, and larger stones are used occasionally. The collapse of the Futamata-Fukura Bridge during the Kumamoto earthquake revealed that soil was used as the filling material in this bridge. In contrast, the Tsujun Bridge, which was designated as a national treasure in 2023 and uses stones as large as wall stones as the filling material, did not collapse during the same earthquake. Based on these observations, the authors considered that the grain size of the filling material affects the seismic performance of stone arch bridges. In the restoration of the collapsed Futamata-Fukura Bridge after the Kumamoto earthquake, split stones were used as the filling material and packed tightly to enhance integration, indicating that engineers assessed that split stones are superior to soil as the filling material. However, research focusing on the filling material size has not been reported to date.

With this background, the authors investigated whether the seismic performance of stone arch bridges can be improved by replacing the filling material with larger stones. To this end, the authors compared the seismic performance of simple wall models with large and small filling materials in a previous study (Higashi *et al*. 2021), and found that the wall with larger filling material withstood larger shaking. However, the experiment did not consider arches nor the actual shape of stone arch bridges. Therefore, this study used three-dimensional stone arch bridges to consider the actual shape of the bridge, and investigated whether the seismic performance of stone arch bridges can be improved by using larger stones as the filling material. Using filling material with larger grain size is less compromising to the cultural value of stone arch bridges compared with employing modern reinforcing materials.

Recent studies on seismic retrofitting of historical structures have focused not only on stone arch bridges but also on other masonry constructions, such as brick and adobe structures. These studies explore the use of advanced materials and techniques that can reinforce structures without compromising their cultural integrity (Corradi *et al*. 2023, Baeza *et al*. 2024, Zhang *et al*. 2021, Yavartanoo and Kang 2022, Güleroğlu *et al*. 2020, Ban *et al*. 2024). These approaches not only enhance seismic performance but also aim to preserve structures for future generations with minimal impact on their heritage values. Moreover, they emphasize sustainability, focusing on reduced carbon dioxide emissions, reversibility, and low energy consumption. Materials such as cross-laminated timber, natural fibers, fiber-reinforced Polymers (FRP) with natural lime coatings, carbon fibers, and textile-reinforced mortars are discussed. Incorporating these recent developments in the field of stone arch retrofit could potentially provide valuable insights for improving the seismic resilience of stone arch bridges while preserving their historical significance.

Previous studies on stone arch bridges include studies that have conducted static loading tests to elucidate the damage mechanisms and bearing capacity under vertical traffic loading (Fujita *et al*. 2013, Hu *et al*. 2020), studies that have taken on-site vibration measurement to elucidate vibration characteristics (Aytulun *et al*. 2022, Bayraktar *et al*. 2015), studies on repair and restoration measures using new materials such as ultrahigh-performance concrete (Wang *et al*.

2022) and carbon fiber reinforced plastic (CFRP) bars (Zhang *et al*. 2023), studies to establish numerical simulation methods using the three-dimensional nonlinear finite element method (FEM) (Mentese *et al*. 2023, Silva *et al*. 2022, Silva *et al*. 2024), studies using probabilistic-based structural assessment based on three-dimensional numerical simulations (Conde *et al*. 2021, Gönen and Soyöz, 2022), and studies using the three-dimensional distinct element method (DEM) (Mehrbod *et al*. 2022, Furukawa *et al*. 2019).

Most experimental studies have considered vertical traffic loading, while few experimental studies have considered earthquake loading. On-site vibration measurement is important for understanding the vibration characteristics, but the seismic performance cannot be understood based on on-site vibration measurement with small vibration amplitude. Therefore, for stone arch bridges, shaking table tests must be conducted to understand the damage mechanism and capacity under earthquake loading.

In the post-earthquake recovery of historic stone arch bridges in Japan, damaged historic stone arch bridges must be restored to their original state to preserve historical heritage. However, integrating new materials poses challenges, because these materials may compromise the historical integrity and cultural significance of stone arch bridges. Therefore, reinforcing methods that do not use new materials are preferable. Regarding reinforcing methods without new materials, the use of interlocking blocks instead of regular blocks has been investigated (Furukawa *et al*. 2022, Furukawa *et al*. 2020). However, although this approach reinforces the wall, it cannot reinforce the filling material. This study aimed to improve the stability of the filling material itself without using new material, but rather by increasing the size of the material, to improve the seismic performance of the entire stone arch bridge.

Numerical simulation is important for understanding the damage mechanism and effectiveness of restoration measures. Because the collapsibility of the filling material affects earthquake damage, the appropriate modeling of the filling material must consider the filling material's discontinuous nature. The DEM models the motion of individual stones, is suitable for analyzing collapse phenomena, and can also model the discontinuous nature of the filling material. Therefore, this study adopted the DEM and modeled each stone independently.

The original DEM using polyhedral elements has the drawback that spring constants cannot be determined based on the material properties. Therefore, the spring constant must be determined empirically or experimentally (Kiyono and Furukawa, 2004; Furukawa and Ohta, 2009), and there are issues with the reliability of the results. This drawback was solved in the refined DEM, where the spring constant can be determined theoretically from the material properties (Furukawa *et al*. 2011). The reliability of the refined DEM has been verified by confirming its ability to reproduce elastic behavior with the same degree of accuracy as the FEM (Furukawa *et al*. 2011) and reproduce failure modes similar to those observed in experiments (Parajuli *et al*. 2020).

In this study, a shaking table test was conducted to elucidate the collapse mechanism and examine the size effect of the filling material on the seismic performance of stone arch bridges.

The seismic performance of two test specimens with large and small filling materials were compared. The two excitation directions, namely, the transverse and longitudinal direction, were also considered, and the collapse behavior for each excitation direction was investigated. Furthermore, shaking table tests were numerically simulated using the three-dimensional refined DEM to better understand the damage mechanism and effect of filling material size on the seismic performance of stone arch bridges. By comparing the seismic performance using the shaking table test and numerical simulation, this study investigated whether the seismic performance of stone arch bridges can be improved by using larger stones as the filling material.

(a) Test specimen placed on shaking table

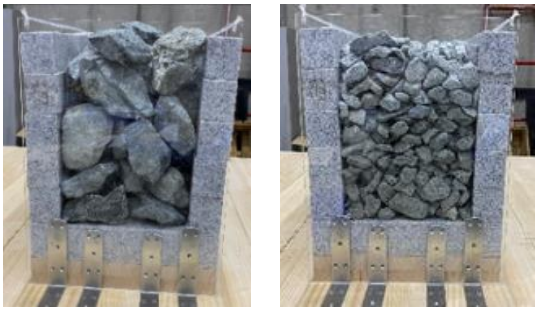

(b)Test specimens with large crushed stones (left) and small crushed stones (right)

Fig. 1 Photos of test specimens

2. Shaking table test

2.1 Test specimens

A photo of a test specimen of the stone arch bridge is shown in Fig. 1(a). This specimen is made of ring stones and wall stones, and employs crushed stones as the filling material. Both the ring stones and wall stones are made of white granite.

Two types of crushed stones, large and small, were used as the filling material. The size of the large crushed stones is approximately 40–100.0 mm, and the size of the small crushed stones is approximately 20–50 mm. Therefore, there are two test specimens: a test specimen with large crushed stones and a test specimen with small crushed stones, as shown in Fig. 1(b).

The same set of crushed stones was used for all excitations, but using the same arrangement of crushed stones was not possible. The volume of the stored crushed stones was estimated based on the density and total weight of the filled crushed stones. Then, the volumetric filling ratio of the crushed stones was calculated as 46% for the model with large crushed stones and 43% for the model with small crushed stones.

As shown in Fig. 1(a), transparent acrylic plates with a thickness of 5 mm were placed on both sides of the test specimen to prevent the crushed stones from collapsing in the side direction, and used to observe the behavior of crushed stones during excitation. The acrylic plates were fixed to the shaking table at the bottom using L-shaped angles. The two acrylic plates were connected at the top with two ropes to prevent outward deflection. In this experiment, the acrylic plates were merely in contact with the spandrel walls and exerted minimal compressive force. Although this setup helps restrain the spandrel walls from opening laterally, it offers limited resistance to out-of-plane collapse. If compressive force were applied to the acrylic plates from both sides, this force would be transferred to the spandrel walls, potentially increasing frictional resistance and improving stability compared to the current setup. Therefore, it is anticipated that the lateral restraint provided by the acrylic plates could influence the collapsibility of the spandrel walls, and this aspect will be explored in future research.

The dimensions of the test specimen are shown in Fig. 2. The test specimen was modelled after the Nigorigawa Bridge in Kumamoto, Japan. In conducting shaking table tests under gravitational acceleration using scaled models made from the same materials as the original structures, it is

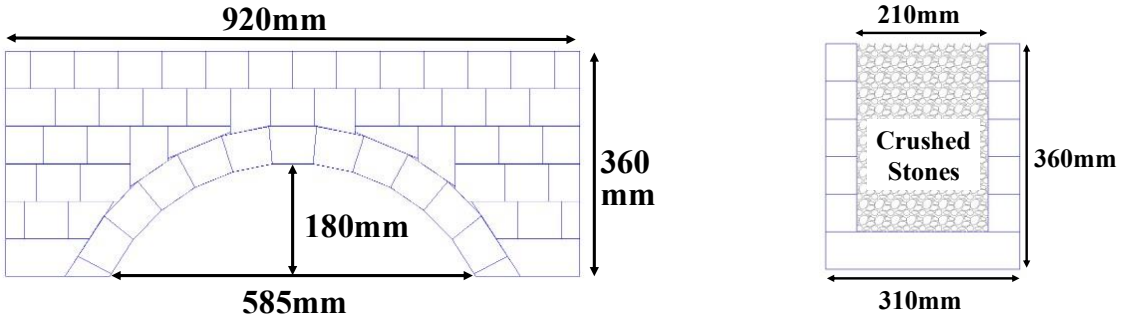

(a) Front view (b) Side view

Fig. 2 Test specimen dimensions

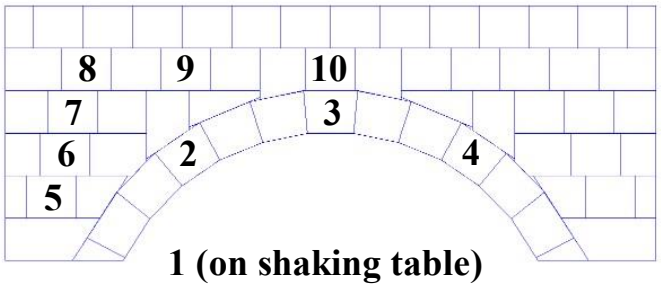

Fig. 3 Location of accelerometers for sweep excitation.

common practice to apply additional mass to the test specimens to satisfy similarity laws. However, additional mass was not applied due to the risk of potential collapse of the test specimens caused by the added mass. Consequently, addressing the similarity law remains a topic for future research.

The shaking table used in this study is a hydraulic servo shaking table manufactured by Shimadzu Corporation. The table size is 1.5 meters by 1.5 meters, with an allowable weight capacity of 20 kN. The table operates in a unidirectional shaking direction, with a maximum displacement of ±100 mm and a maximum acceleration of ±2 G.

Two types of experiments were conducted: sweep excitation and sine wave excitation. Excitation was applied in two directions, namely, the transverse and longitudinal direction. The accelerometer locations for sweep excitation are shown in Fig. 3. Accelerometer No. 1 was installed on the shaking table, accelerometers No. 2–4 were attached to the ring stones, and accelerometers No. 5–10 were attached to the wall stones. The acceleration in the excitation direction was measured. In the case of sine wave excitation, the accelerometers No. 2-10 were removed from the test specimen because they could affect the failure behavior.

2.2 Sweep excitation

2.2.1 Method

First, sweep excitation was conducted to understand the vibration characteristics and natural frequencies of the test specimen. The test specimens were excited with an acceleration amplitude

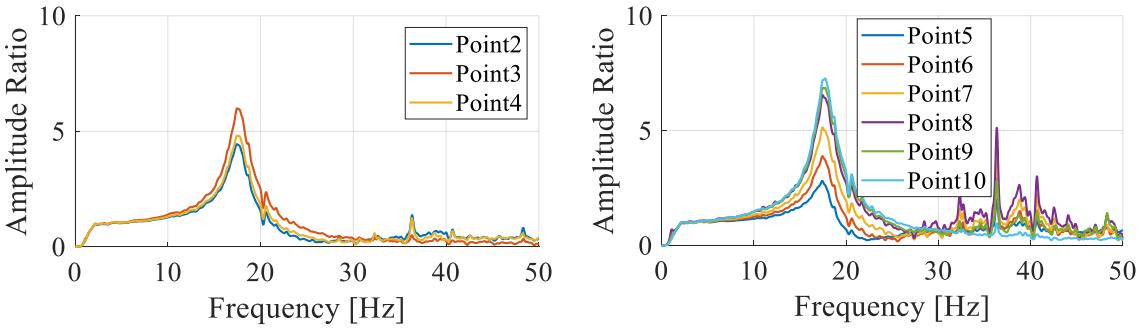

(a) Stone arch bridge with large crushed stones (left: measured at ring stones; right: measured at wall stones)

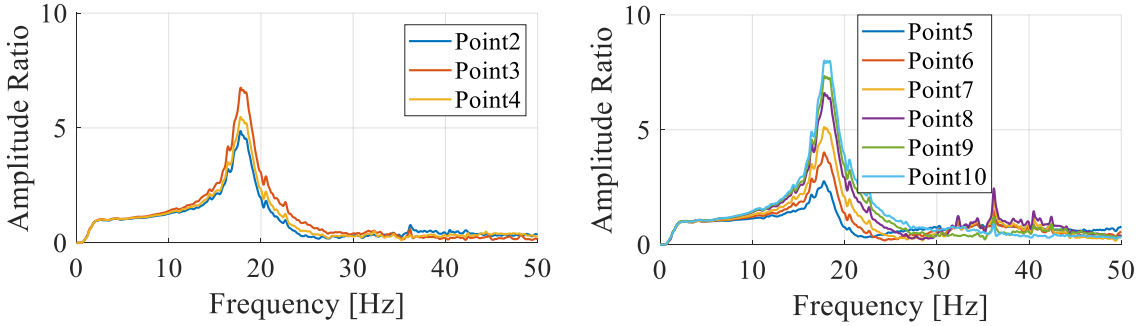

(b) Stone arch bridge with small crushed stones (left: measured at ring stones; right: measured at wall stones)

Fig. 4 Resonance curve of test specimen in transverse direction

that was sufficiently small to prevent the collapse of the test specimens, and the excitation frequency was gradually increased. The resonant curves were obtained by taking the ratio of the acceleration Fourier spectrum measured at the stones (Accelerometers No. 2–10) to the acceleration Fourier spectrum measured on the shaking table (Accelerometer No. 1). The natural frequencies of the test specimen were estimated by reading the dominant frequencies of the resonance curves. Here, the dominant frequency estimated by the sweep excitation with a small acceleration amplitude is called the natural frequency.

2.2.2 Result

Fig. 4 shows the resonance curves of the test specimen with large and small crushed stones in the transverse direction. Fig. 5 shows the resonance curves of the test specimen with large and small crushed stones in the longitudinal direction. The left figures show the resonance curves measured at the ring stones, while the right figures show the resonance curves measured at the wall stones. The point number indicates the accelerometer numbers shown in Fig. 3.

By comparing Figs. 4(a) and 4(b), and comparing Figs. 5(a) and 5(b), it can be found that the stone arch bridges have similar resonant curves and similar natural frequencies regardless of the size of crushed stones. The fact that the two test specimens have the similar natural vibration characteristics suggests that the size of the crushed stones, not its vibration characteristics, may have an effect on the collapsibility of the two test specimens when their collapsibility is different.

Additionally, it was found that the arch and wall vibrate as a unified body, because a similar natural frequency was observed regardless of the measurement points.

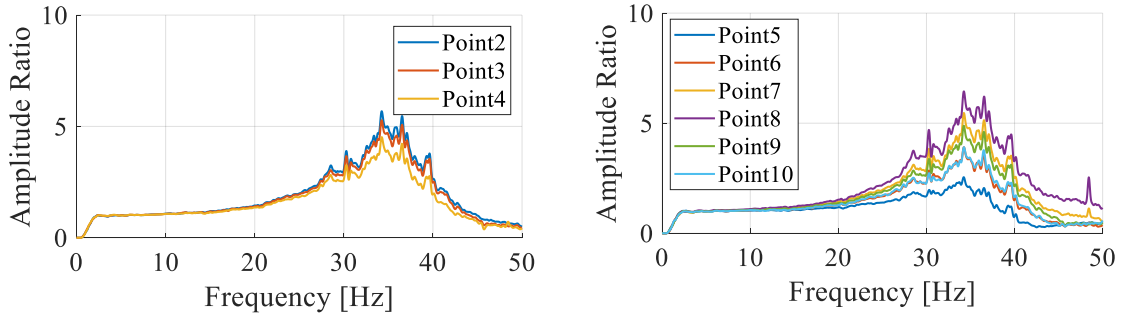

(a) Stone arch bridge with large crushed stones (left: measured at ring stones; right: measured at wall stones)

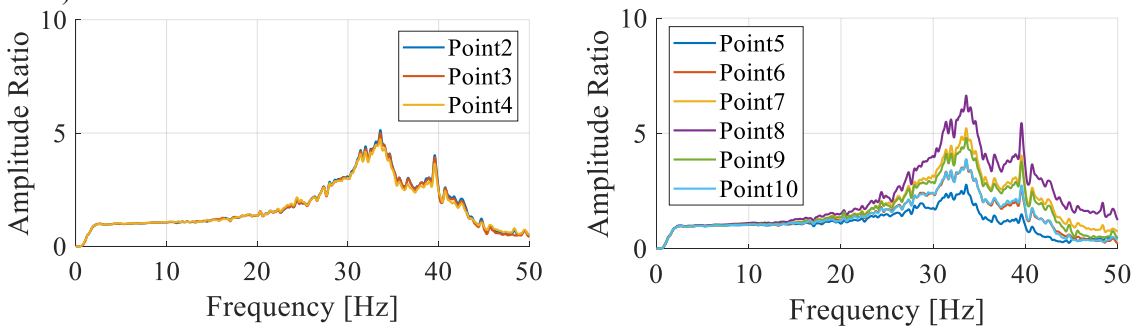

(b) Stone arch bridge with small crushed stones (left: measured at ring stones; right: measured at wall stones)

Fig. 5 Resonance curve of test specimen in longitudinal direction

Table 1 Natural frequency of stone arch bridge with large and small crushed stones by sweep excitation

Direction	Transverse	Longitudinal
Large crushed stones	17.3 Hz	33.8 Hz
Small crushed stones	17.8 Hz	33.5 Hz

Table 1 summarizes the natural frequencies of the two test specimens with large and small crushed stones in the two directions.

2.3 Sine wave excitation

2.3.1 Method

Next, sine wave excitation was carried out. The test specimens were excited by a sine wave with constant frequency and acceleration amplitude up to collapse. The collapse behavior and time to collapse were observed. It is also possible to evaluate seismic resistance by comparing the level of acceleration at which collapse occurs, rather than the time to collapse. However, since the collapse depends on both the level of acceleration and the duration of the excitation, this study simply compared the time to collapse after excitation at a constant acceleration.

In each direction, two excitation frequencies were selected: the natural frequency (17 Hz for the transverse direction and 33 Hz for the longitudinal direction) and 6 Hz, which is far from the natural frequency. 6 Hz was selected as one example of an excitation frequency away from the natural frequency. Because the resonance curve is similar between the two test specimens with large and small crushed stones (Figs. 4 and 5), the difference in the vibration characteristics is considered to be negligible and the effect of the crushed stone size on the collapse of stone arch bridges can be observed.

(a) Stone arch bridge with large crushed stones excited by sine wave with frequency of 6 Hz and amplitude of 150 gal

(b) Stone arch bridge with small crushed stones excited by sine wave with frequency of 6 Hz and amplitude of 150 gal

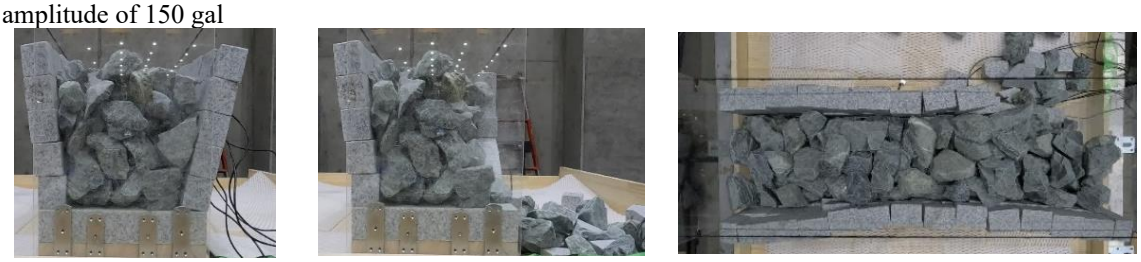

(c) Stone arch bridge with large crushed stones excited by sine wave with frequency of 17 Hz and amplitude of 75 gal

(d) Stone arch bridge with small crushed stones excited by a sine wave with frequency of 17 Hz and amplitude of 75 gal

Fig. 6 Collapse behavior of test specimen excited by sine wave in transverse direction (left: side view during collapse, middle: side view after collapse, right: view after collapse from above)

2.3.2 Result

Fig. 6 shows the collapse behavior of the test specimens in the transverse direction. The sine wave with 6 Hz and 150 gal, and the sine wave with 17 Hz and 75 gal were input. The left figures show the side view during collapse, the middle figures show the side view after collapse, and the right figures show the top view after collapse. The wall stones and crushed stones collapsed at the side end. The collapse mechanism was the same regardless of the crushed stone size. The crushed stones first collapsed while moving obliquely downward, and then the collapsed crushed stones pushed the wall stones outward, leading to the collapse of the entire stone arch bridge. This finding suggests that the collapsibility of crushed stones is an important factor controlling the collapsibility of stone arch bridges. The collapse did not occur at the center, and only occurred at the side end, because the crushed stones are more likely to collapse at the side end where the amount of crushed stones is large and easier to collapse, and also because the lateral restraint by the acrylic plate is not strong. The influence of the lateral restraint is an issue to be addressed in the future study.

Fig. 7 shows the collapse behavior of the test specimens caused by the sine wave excitation in the longitudinal direction. The sine wave with 6 Hz and 250 gal and that with 33 Hz and 150 gal were input. A similar collapse mechanism was observed regardless of the excitation direction.

Differences in the size of the crushed stones are evident in the shape of the crushed stones after collapse. As shown in the middle figures of Figs. 6 and 7, the post-collapse sloping surface of the crushed stones is steeper for larger crushed stones and gentler for smaller ones. Larger crushed stones were more stable because they are freestanding at a steeper slope angle.

Fig. 8 compares the time to collapse between the test specimens with large and small crushed stones. In all excitations, the test specimen with large crushed stones collapsed later than the test specimen with small crushed stones. Therefore, stone arch bridges with larger crushed stones have better seismic performance.

The observed collapse mechanism emphasizes that the stability of crushed stones controls the stability of the stone arch bridge. Larger crushed stones were more stable, as observed with a steeper slope angle, and their time to collapse was longer. A potential explanation for the stability of larger crushed stones is shown in Fig. 9. Figs. 9(a) and 9(b) compares the situation wherein the two bottom stones are fixed, and the same lateral displacement is applied to the two stones above. In the case of larger stones (Fig. 9(a)), the top right stone does not overturn because its gravity center is above the right bottom stone. However, in the case of smaller stones (Fig. 9(b)), the top right stone overturns because its gravity center is outside the right bottom stone.

Under the same inertia force by earthquake excitation, a similar sliding displacement of the crushed stone is expected, regardless of the crushed stone size. In this situation, larger crushed stones are expected to be more stable, as shown in Fig. 9. Notably, actual crushed stones are not rectangular. However, for the sake of simplicity, rectangular elements were used to provide an explanation.

Therefore, it is possible that the seismic performance of stone arch bridges can be improved simply by increasing the size of the filling material.

Due to limitations in the shaking table and control system, the current setup is restricted to simplified waveforms, such as sinusoidal inputs. However, incorporating other types of excitations, such as scaled real earthquake records like the Kobe or El-Centro earthquakes, would provide deeper insights into the behavior of the stone arch bridge. In future work, the use of realistic earthquake waveforms through potential equipment upgrades or advanced numerical simulations is intended to better understand the seismic response of the structure.

(a) Stone arch bridge with large crushed stones excited by sine wave with frequency of 6 Hz and amplitude of 250 gal

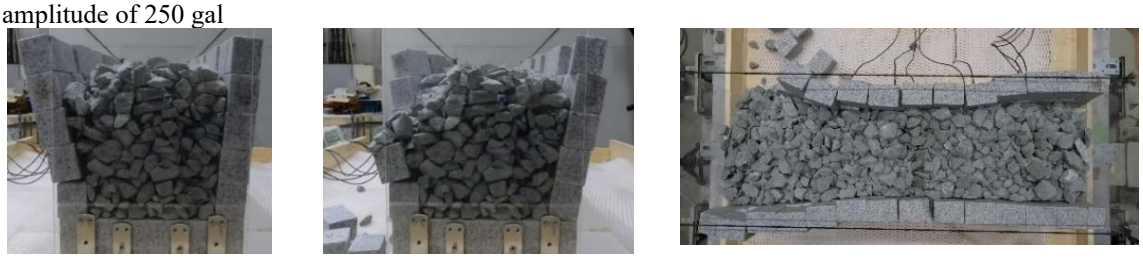

(b) Stone arch bridge with small crushed stones excited by sine wave with frequency of 6 Hz and amplitude of 250 gal

(c) Stone arch bridge with large crushed stones excited by sine wave with frequency of 33 Hz and amplitude of 150 gal

(d) Stone arch bridge with small crushed stones excited by sine wave with frequency of 33 Hz and amplitude of 150 gal

Fig. 7 Collapse behavior of test specimen excited by sine wave in longitudinal direction (left: side view during collapse; middle: side view after collapse; right: view after collapse from above)

3. Numerical Investigation

3.1 Refined DEM

Next, the effect of the size of the filling material was investigated numerically by simulating the shaking table tests using the refined DEM (Furukawa *et al*. 2011). The refined DEM models a

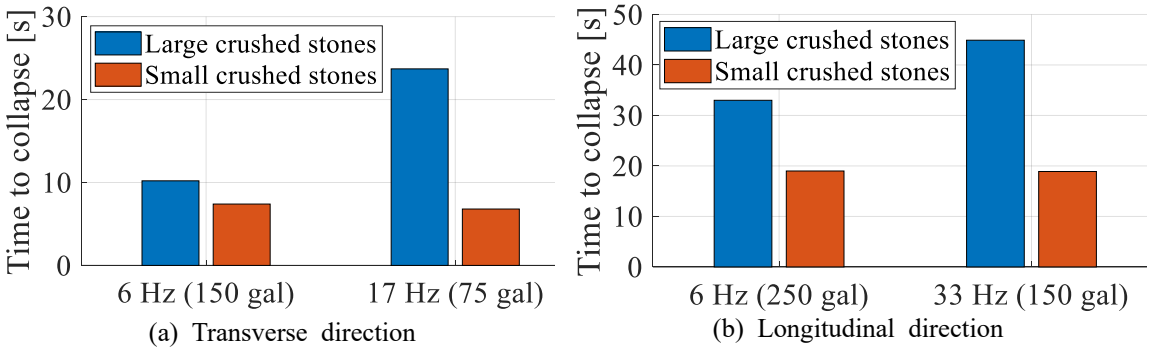

Fig. 8 Comparison between time to collapse of test specimens with large and small crushed stones

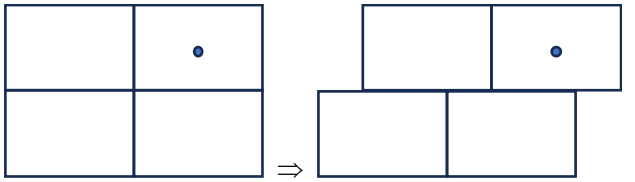

(a) Large stones

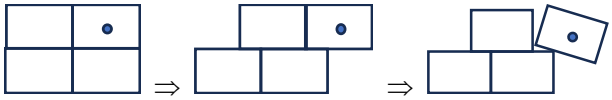

(b) Small stones

Fig. 9 Movement of two top stones under same lateral movement (the two bottom stones are fixed)

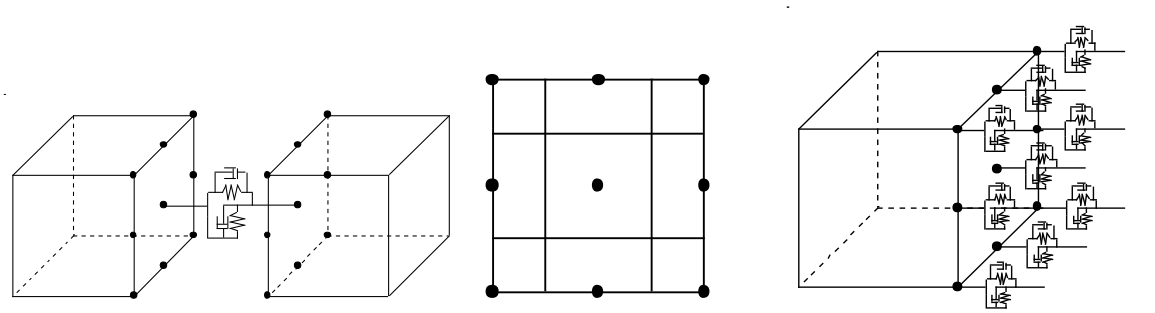

(a) Spring and dashpot (b) Segments and contact points (c) Multiple springs and dashpots

Fig. 10 Basic concept of the refined DEM (Furukawa *et al.* 2011)

structure as an assembly of rigid elements, and the interaction between elements is modeled using springs and dashpots, as in the original DEM. The point of difference to the original DEM is that the spring constant is theoretically determinable from the material properties. Therefore, there is no need to determine the spring constant by trial and error, as in the original DEM.

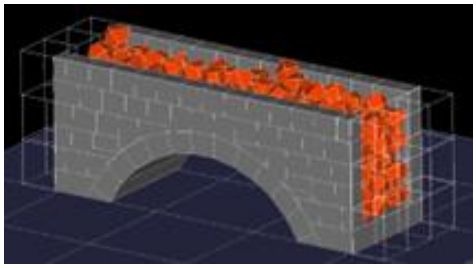

(a) Numerical model of test specimen

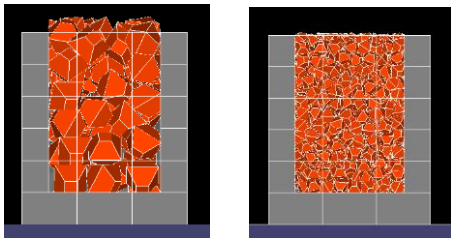

(b) Numerical models of test specimens with large crushed stones (left) and small crushed stones (right)

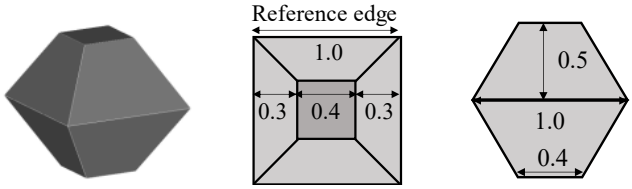

(c)Numerical model of crushed stones

Fig. 11 Numerical model of test specimen.

Fig. 10(a) shows a spring and dashpot used for computing the contact force between elements in contact. The dashpot is introduced to represent energy dissipation due to the contact. The surface of each element is divided into small segments, as shown in Fig. 10(b). The black points indicate the representative point of each segment, and the contact force between elements is computed at these points. A combination of a spring and a dashpot is attached to each segment at these representative points, as illustrated in Fig. 10(c). The spring constant for each segment, per segment area, is derived from the stress-strain relationship of the material. When elements *A* and *B* are in contact, springs are set in both the normal and shear (tangential) directions on the contact surface. The spring constants per area in the normal and shear directions, denoted as k_n and k_s, are calculated as follows

$$k_n = \frac{1}{\frac{L_A}{E_A/(1-\nu_A{}^2)} + \frac{L_B}{E_B/(1-\nu_B{}^2)}} \qquad k_s = \frac{1}{\frac{L_A}{E_A/(1+\nu_A)} + \frac{L_B}{E_B/(1+\nu_B)}} \tag{1}$$

where E is Young's modulus, ν is Poisson's ratio, and L is the distance from the gravity center to the surface at which the spring is connected. The subscripts A and B indicate the value for the elements A and B in contact. The forces acting on each element are computed by summing the contact force, along with external forces such as gravitational force and inertial force of an earthquake. The translational and rotational behavior of each element are calculated explicitly by solving Newton's law of motion and Euler's equation of motion. Further details can be found in reference (Furukawa *et al*. 2011).

3.2 Numerical model

The numerical model is shown in Fig. 11(a). The individual ring stones and wall stones were modeled by single hexahedral elements and are shown in gray. The individual crushed stones were

(a) Illustration of angle of repose measurement

(b)Illustration of friction force measurement

Fig. 12 Illustration of coefficient of friction measurement.

modeled using single decahedral elements and shown in red. Each acrylic plate was modeled as an assembly of rectangular elements and is shown as transparent. The shaking table was modeled as an assembly of rectangular elements and is shown using purple elements. Two numerical models with large and small crushed stones were prepared, as shown in Fig. 11(b). Fig. 11(c) shows the decahedral element that was used to model the crushed stone. The ratio of each edge length to the reference edge length was fixed, as shown in Fig. 11(c). The reference edge length of large crushed stones is 60 mm, and that of small crushed stones is 25 mm, based on the average size of the crushed stones used in the shaking table tests. Although actual crushed stones have variable size and shape, the numerical simulation in this study considered uniform crushed stones.

The crushed stone elements were filled inside the wall stones by free fall. A total of 119 large crushed elements and 2526 small crushed stone elements were filled. A similar volumetric filling ratio of the crushed stones to the shaking table test was realized, which was 46% for the model with large crushed stones and 43% for the model with small crushed stones.

Regarding the boundary conditions, the shaking table and acrylic plates were fixed. The acceleration history of the shaking table was input into the gravity center of the ring stones, wall stones, and crushed stones as the inertia force.

3.3 Material properties and friction coefficient

The material properties used in the simulation are listed in Table 2. Young's modulus of the ring stones, wall stones, and crushed stones was assumed to be the same determined such that the natural frequency in the transverse direction of the numerical model matched the experimental value. The density of each material was measured, and the Poisson's ratio of each material and the Young's modulus of the acrylic plate were determined based on the general values.

The friction coefficients between the two materials are listed in Table 3. The coefficients of friction between each material and the crushed stones were determined such that the angle of repose of the numerical simulation and the experiment (Fig. 12(a)) were in agreement. The coefficients of friction between each material and the ring and wall stones were estimated using a spring scale as shown in Fig. 12(b).

3.4 Resonant curve and natural frequencies

First, the sweep excitation was simulated. Acceleration was applied to the gravity center of each element as the inertia force. Additionally, gravitational force was applied to the gravity center of each element.

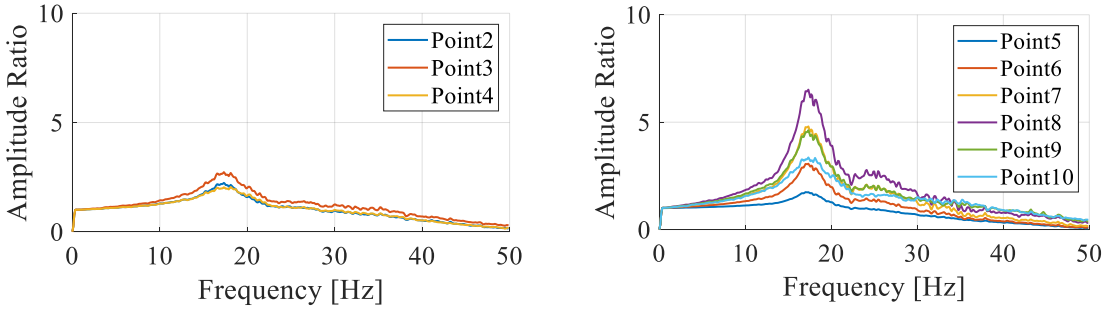

(a) Stone arch bridge with large crushed stones (left: simulated at ring stones; right: simulated at wall stones)

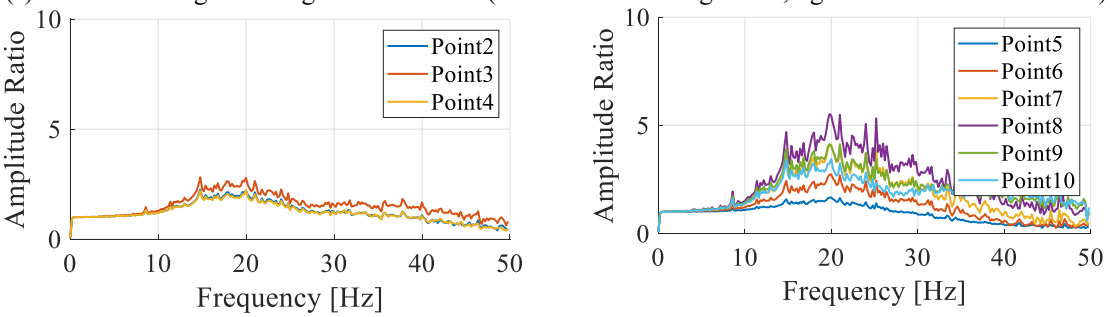

(b) Stone arch bridge with small crushed stones (left: simulated at ring stones; right: simulated at wall stones)

Fig. 13 Resonance curve of numerical model in transverse direction

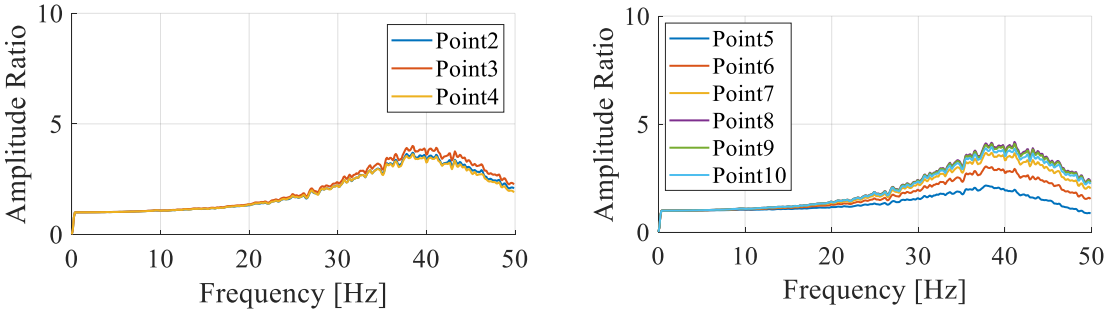

(a) Stone arch bridge with large crushed stones (left: simulated at ring stones; right: simulated at wall stones)

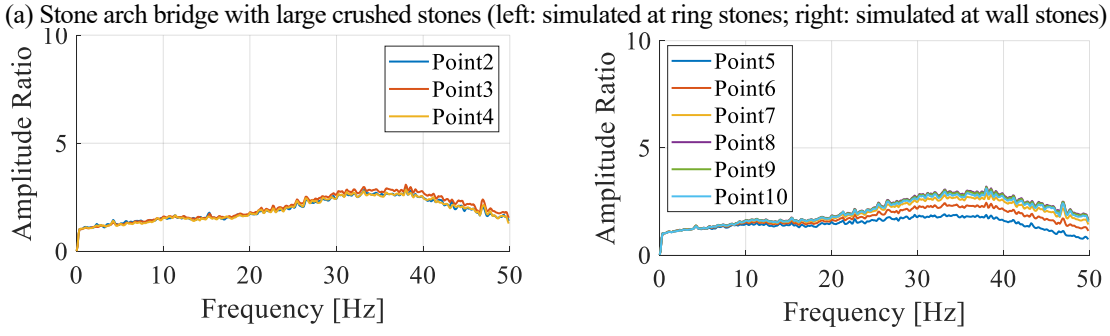

(b) Stone arch bridge with small crushed stones (left: simulated at ring stones; right: simulated at wall stones)

Fig. 14 Resonance curve of numerical model in transverse direction

Table 2 Material properties

Material	Density (t/m^3)	Young's modulus (N/m^2)	Poisson's ratio
Ring stone/Wall stone	2.20	8.0×10^7	0.25
Crushed stone	3.20	8.0×10^7	0.25
Acrylic plate	1.19	3.0×10^9	0.35

Table 3 Friction coefficient between two materials

	Ring stone/ Wall stone	Crushed stone	Acrylic plate	Wood plate on shaking table
Ring stone/Wall stone	0.666	0.772	0.279	0.516
Crushed stone	0.772	0.2	0.152	0.707

Fig. 13 shows the computed resonant curves in the transverse direction. By comparing Figs. 4 and 13, it can be found that the numerical simulation could not reproduce the amplitude of the resonance curves around the natural frequencies. However, the natural frequency of 17 Hz and amplitude ratio at 6 Hz were reproduced. Fig. 14 shows the computed resonant curves in the longitudinal direction. By comparing Fig. 5 to Fig. 14, it can be found that the resonant curves of the numerical simulation were dominant around 38 Hz, which is slightly higher than the experimental natural frequency of 33 Hz. The numerical simulation could not reproduce the resonance curve perfectly, but could reproduce the amplitude ratio of the resonance curves at 6 Hz.

3.5 Sine wave excitation

A numerical simulation of sine wave excitation was also conducted. A sine wave with a constant frequency and constant acceleration was input into the gravity center of each element in the form of inertia force. The gravity force was also input.

In the transverse direction, a sine wave with 6 Hz and 150 gal, and a sine wave with 17 Hz and 600 gal were input. When the sine wave with 17 Hz and 75 gal was input, collapse did not occur. Therefore, a sine wave with 17 Hz and 600 gal was input to observe the collapse behavior. In the longitudinal direction, a sine wave with 6 Hz and 250 gal, and a sine wave with 33 Hz and 700 gal were input. When the sine wave with 33 Hz and 200 gal was input, collapse did not occur. Therefore, a sine wave with 33 Hz and 700 gal was input. For collapse to occur with shaking at 17 Hz and 33 Hz, the numerical analysis required higher accelerations compared with the experiment. The reason for this is that the reproducibility around the natural frequencies was not high, as suggested by the low reproducibility of the resonance curves around the natural frequencies.

Fig. 15 shows the collapse behavior of the numerical model excited by a sine wave in the transverse direction. The left figures show the side views during collapse, the middle figures show the side views after collapse, and the right figures show the top views after collapse. More crushed stones collapsed and scattered in the model when using small crushed stones, and the amount of crushed stones that did not collapse was greater in the model with larger crushed stones, indicating a tendency similar to that in the shaking table tests.

The displacement distribution contours at the time of collapse (approximately 1s before collapse) are shown in Fig. 16. Because a similar tendency was observed in all cases, regardless of

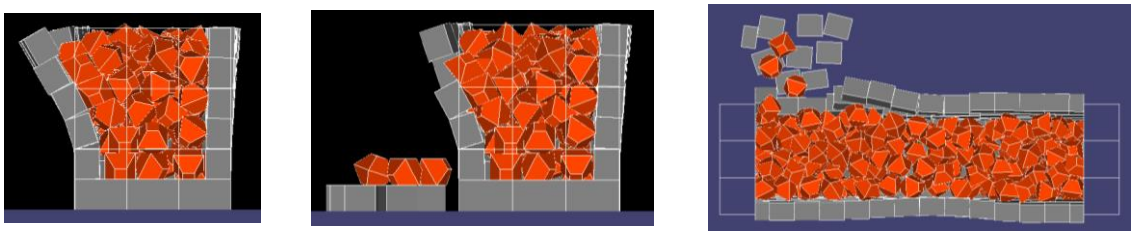

(a) Stone arch bridge with large crushed stones excited by sine wave with frequency of 6 Hz and amplitude of 150 gal

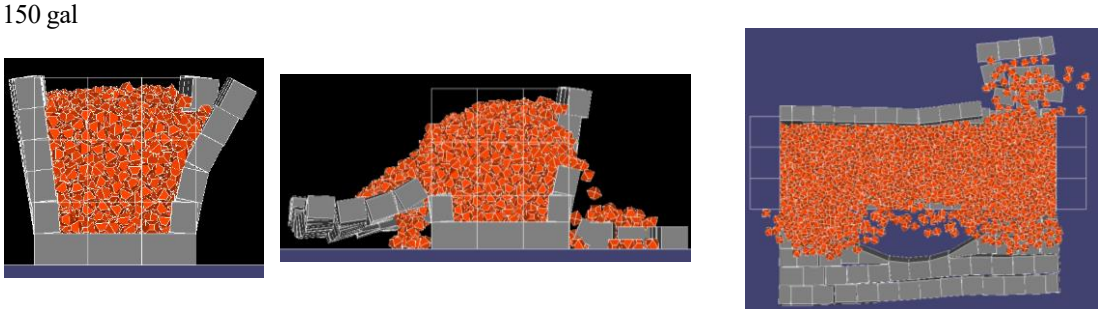

(b) Stone arch bridge with small crushed stones excited by sine wave with frequency of 6 Hz and amplitude of 150 gal

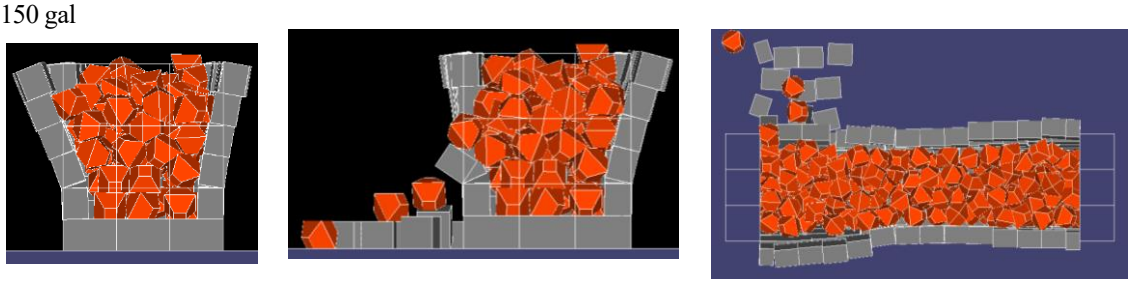

(c) Stone arch bridge with large crushed stones excited by sine wave with frequency of 17 Hz and amplitude of 75 gal

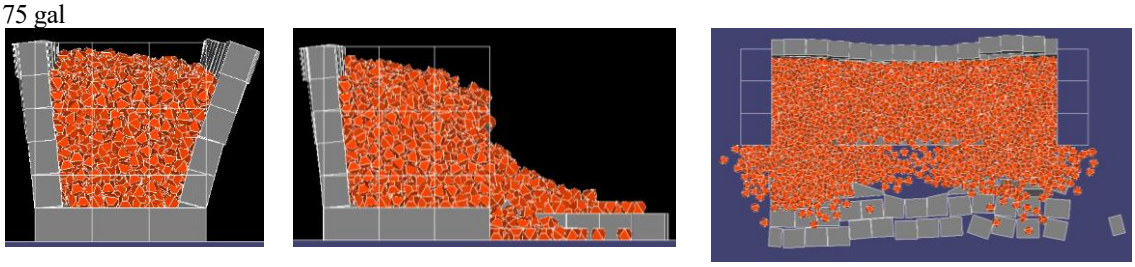

(d) Stone arch bridge with small crushed stones excited by sine wave with frequency of 17 Hz and amplitude of 75 gal

Fig. 15 Collapse behavior of numerical model excited by sine wave in transverse direction (left: side view during collapse; middle: side view after collapse; right: top view after collapse)

the crushed stone size and the excitation direction and frequencies, only the case wherein the numerical model with small crushed stones was excited with a sine wave of 17 Hz and 600 gal in the transverse direction is shown. Figure 16(a) shows the settlement displacement and Fig. 16(b) shows the lateral displacement in the transverse direction. As shown in Fig. 16(a), the large vertical settlement of crushed stones occurred at both side ends of the stone arch bridge, whereas

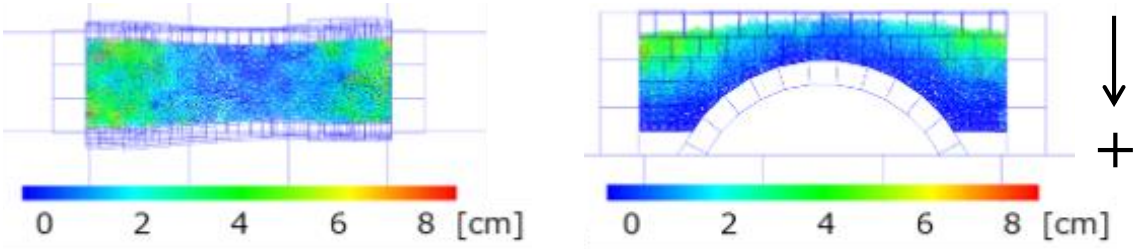

(a) Settlement displacement (left: top view; right: front view)

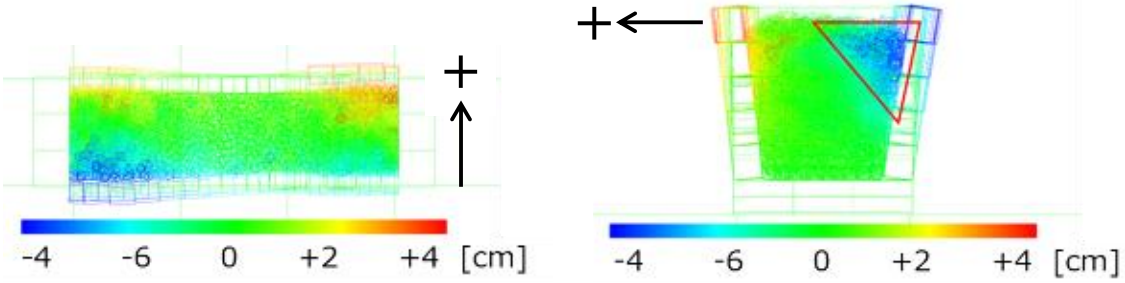

(b) Lateral displacement in transverse direction (left: top view; right: side view)

Fig. 16 Displacement of numerical model with small crushed stones after excitation with 17 Hz and 600 gal

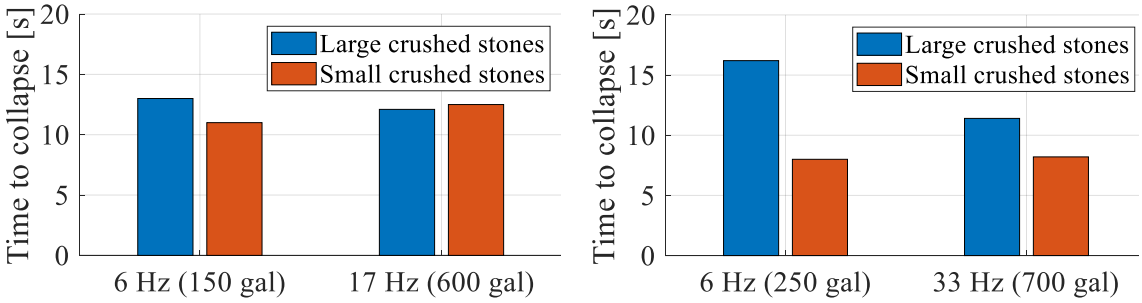

(a) Transverse direction (b) Longitudinal direction

Fig. 17 Comparison of time to collapse between numerical models with large and small crushed stones

little vertical settlement was observed at the arch center. The right figure of Fig. 16(b) shows that the triangular area of the crushed stones moved and pushed the wall outward. These findings support the collapse mechanism whereby the filling material collapses and pushes the wall, leading to total collapse. Because both side ends had a larger amount of crushed stones, collapse occurred easily at both sides. Therefore, large displacement and failure occurred at the side ends.

Fig. 17 compares the time to collapse of the numerical models with large and small crushed stones. Except for the case with 17 Hz in the transverse direction, the numerical model with large crushed stones collapsed later compared with the model with small crushed stones. Specifically, the difference in the time to collapse was larger in the longitudinal direction, which is similar to the experimental results (Fig. 8). In the case of a sine wave with 17 Hz and 600 gal, the model with small crushed stones collapsed later than the model with large crushed stones, possibly because the natural frequency of the model with small crushed stones was further away from 17

Hz compared with the model with large crushed stones, as shown in Fig. 14.

The above findings suggest that the stone arch bridge with larger crushed stones has better seismic performance. Hence, in the maintenance and management of stone arch bridges, using filling material with larger size is expected to improve the seismic performance.

4. Conclusions

This study conducted shaking table tests and numerical simulations using the refined DEM to investigate whether the seismic performance of stone arch bridges can be improved by using filling material with larger stones.

In the shaking table tests, two stone arch bridge specimens were tested: one filled with large crushed stones and another one filled with small crushed stones. The test specimens were excited in the transverse and longitudinal direction.

First, sweep wave excitation was applied to measure the natural frequencies of the test specimens, and it was found that the natural frequencies and resonance curves were approximately identical, regardless of the crushed stone size, in both directions.

Then, sine wave excitation with constant frequency and acceleration amplitude was applied until the test specimen collapsed. In all cases, the test specimen with larger crushed stones collapsed later. The failure mechanism was as follows: the filling material collapsed, pushed the wall, and led to the total collapse of the wall stones and crushed stones. Collapse occurred at the side edge and not at the arch center. The same failure mechanism was observed regardless of the crushed stone size, excitation direction, and excitation frequencies. The post-collapse sloping surface of the larger crushed stones was steeper, suggesting that larger crushed stones are stable. Therefore, the collapsibility of the filling material itself is important, and the test specimen with larger crushed stones resisted the shaking for longer time.

In the numerical simulation of sine wave excitation, a failure mechanism similar to that of the shaking table tests was observed, regardless of the crushed stone size, excitation direction, and excitation frequencies. The numerical model with larger crushed stones collapsed later than that with small crushed stones, except for one case wherein the model was excited with 17 Hz in the transverse direction and collapsed earlier.

Through shaking table tests and numerical simulations, this study observed that larger crushed stones are more stable, the stability of the filling material is an important factor controlling the collapsibility of stone arch bridges, and stone arch bridges with large crushed stones can resist earthquake shaking for longer time. These results suggest that stone arch bridges with larger crushed stones have better seismic performance. Therefore, in the maintenance and management of stone arch bridges, using filling material with larger size can improve seismic performance.

Acknowledgments

This study was supported by JSPS KAKENHI Grant Number 23H01658. We thank Edanz (https://jp.edanz.com/ac) for editing a draft of this manuscript.

References

Aytulun, E., Soyoz, S. and Karcioglu, E. (2022), "System identification and seismic performance assessment of a stone arch bridge", *J. Earthq. Eng.*, **26**(2), 723-743. https://doi.org/10.1080/13632469.2019.1692740.

Ban, S., Shrestha, K.C. and Bastola, S. (2024), "Seismic performance assessment of stone masonry buildings: Efficacy of various strengthening elements", *J. Build. Eng.*, **96**(110380), https://doi.org/10.1016/j.jobe.2024.110380.

Bayraktar, A., Türker, T. and Altunişik, A.C. (2015), "Experimental frequencies and damping ratios for historical masonry arch bridges", *Constr. Build. Mater.*, **75**, 234-241. https://doi.org/10.1016/j.conbuildmat.2014.10.044.

Baeza, F.J., Estevan, L. and Ivorra, S. (2024), "Seismic retrofitting of heritage structures, actual techniques and future challenges for earth and masonry constructions", (Eds., Endo, Y. and Hanazato, T.), Structural Analysis of Historical Constructions, *RILEM Bookseries*, **47**, 1088-1101. Springer, Cham. https://doi.org/10.1007/978-3-031-39603-8_87.

Conde, B., Matos, J.C., Oliveira, D.V. and Riveiro, B. (2021), "Probabilistic-based structural assessment of a historic stone arch bridge", *Struct. Infrastruct. Eng.*, **17**(3), 379-391. https://doi.org/10.1080/15732479.2020.1752261.

Corradi, M., Mustafaraj, E. and Speranzini, E. (2023), "Sustainability considerations in remediation, retrofit, and seismic upgrading of historic masonry structures", *Environ. Sustain. Remediation*, **30**, 25274-25286. https://doi.org/10.1007/s11356-021-17490-7.

Gönen, S. and Soyöz, S. (2022), "Reliability-based seismic performance of masonry arch bridges", *Struct. Infrastruct. Eng.*, **18**(12), 1658-1673. https://doi.org/10.1080/15732479.2021.1918726.

Fujita, C., Yamao, T., Koga, K. and Ogura, M. (2013). "Static behavior by stone arch model and mechanism of cracking of arch ring stone", *J. Struct. Eng.*, **59**, 26-36. (in Japanese).

Furukawa, A., Kiyono, J. and Toki, K. (2011), "Proposal of a numerical simulation method for elastic, failure and collapse behaviors of structures and its application to seismic response analysis of masonry walls", *J. Disaster Res.*, **6**(1), 51-69. http://dx.doi.org/10.20965/jdr.2011.p0051.

Furukawa, A., Masuda, K. and Kiyono, J. (2020), "Diagonal compression test of mortar interlocking masonry walls with various block shapes and different support conditions", *Front. Built Environ.*, **6**(579366), 1-15. http://dx.doi.org/10.3389/fbuil.2020.579366.

Furukawa, A., Prasetyo, J.J. and Kiyono, J. (2022), "Performance of interlocking brick walls against out-of-plane excitation, *Int. J. Geomate*, **22**(89), 100-105. https://doi.org/10.21660/2022.89.gxi413.

Furukawa, A. and Ohta, Y. (2009), "Failure process of masonry buildings during earthquake and associated casualty risk evaluation", *Nat. Hazards*, **49**, 25-51. https://doi.org/10.1007/s11069-008-9275-x.

Furukawa, A., Yoshikawa, H. and Kiyono, J. (2019), "Investigation of the Tsujun Bridge damage mechanism during the 2016 Kumamoto earthquake", *J. Japan Soc. Nat. Disaster Sci.*, **38**(6), 1-23. https://doi.org/10.24762/jndsj.38.S06_1.

Güleroğlu, S.K., Karagüler, M.E., Kahraman, İ. and Umdu, E.S. (2020), "Methodological approach for performance assessment of historical buildings based on seismic, energy and cost performance: A Mediterranean case", *J. Build. Eng.*, **31**(101372), https://doi.org/10.1016/j.jobe.2020.101372.

Higashi, Y., Furukawa, A. and Kiyono, J. (2021), "Fundamental study on relation between filling material size and seismic performance of stone bridges", *J. Japan Soc. Nat Disaster Sci.*, **40**(8), 67-80. https://doi.org/10.24762/jndsj.40.S08_67 (in Japanese).

Hu, C., Luo, W. and Chen, S. (2020), "Evaluation of bearing capacity of reinforced stone arch bridge based on static load test", *IOP Conference Series: Earth and Environmental Science*, **546**(042056). https://doi.org/10.1088/1755-1315/546/4/042056.

Japan Society of Civil Engineers. (2017), "Report on the damage surveys and investigations following the 2016 Kumamoto Earthquake", Maruzen, Tokyo, Japan.

Kiyono, J. and Furukawa, A. (2004), "Casualty occurrence mechanism in the collapse of timber-frame houses during an earthquake", *Earthq. Eng. Struct. D.*, **33**, 1233-1248. http://dx.doi.org/10.1002/eqe.402.

Mehrbod, A., Behnamfar, F., Aziminejad, A. and Hosseini, H.H. (2022), "Seismic vulnerability assessment of stone arch bridges by nonlinear dynamic analysis using discrete element method", *Int. J. Architect. Heritage*, **17**(11), 1791-1812. https://doi.org/10.1080/15583058.2022.2071182.

Mentese, V.G., Gunes, O., Celik, O.C.., Gunes, B., Avsin, A. and Yaz, M. (2023), "Experimental collapse investigation and nonlinear modeling of a single-span stone masonry arch bridge", *Eng. Fail. Anal.*, **152**(107520). https://doi.org/10.1016/j.engfailanal.2023.107520.

Nigeme, E. and Yoshihara, S. (2001), "On misunderstanding about masonry-arch bridges and their environmental features", *Historical studies in Civil Engineering*, **21**, 271-278. https://doi.org/10.2208/journalhs1990.21.271.

Parajuli, R.R., Furukawa, A. and Gautam, D. (2020), "Experimental characterization of monumental brick masonry in Nepal", *Structures*, **28**, 314-1321. https://doi.org/10.1016/j.istruc.2020.09.065.

Silva, R., Costa, C. and Arêde, A. (2022), "Numerical methodologies for the analysis of stone arch bridges with damage under railway loading", *Structures*, **39**, 573-592. https://doi.org/10.1016/j.istruc.2022.03.063.

Silva, R., Ribeiro, D., Costa, C., Arêde, A. and Calçada, R. (2024), "Experimental validation of a non-linear train-track-bridge dynamic model of a stone arch railway bridge under freight traffic", *Int. J. Rail Transport.*, **12**(1), 102-133. https://doi.org/10.1080/23248378.2022.2133783.

Wang, Z., Yang, J., Zhou, J., Yan, K., Zhang, Z. and Zou, Y. (2022), "Strengthening of existing stone arch bridges using UHPC: Theoretical analysis and case study", *Structures*, **43**, 805-821. https://doi.org/10.1016/j.istruc.2022.06.055.

Yavartanoo, F. and Kang, T.H.K. (2022), "Retrofitting of unreinforced masonry structures and considerations for heritage-sensitive constructions", *J. Build. Eng.*, **49**(103993), https://doi.org/10.1016/j.jobe.2022.103993.

Zhang, K., Li, D., Shen, X., Hou, W., Li, Y. and Xue, X. (2023), "Research on strengthening stone arch bridge with CFRP rebars", *Int. J. Build. Pathology Adaptation*, **41**(5), 1014-1028. https://doi.org/10.1108/IJBPA-07-2021-0097.

Zhang, R., Wu, M., Lu, W., Li, X. and Lu, X.. (2021), "Seismic retrofitting of a historic building by using an isolation system with a weak restoring force", *Soil Dyn. Earthq. Eng.*, **148**(106836), https://doi.org/10.1016/j.soildyn.2021.106836.

JK